energies

MDPI

Article

On the Evolution of the Integral Time Scale within Wind Farms

Huiwen Liu [1,2], Imran Hayat [3], Yaqing Jin [2] and Leonardo P. Chamorro [2,3,4]*

1 College of Water Conservancy and Hydropower Engineering, Hohai University, Nanjing 210024, China; huiwen_liu@hhu.edu.cn
2 Mechanical Science and Engineering, University of Illinois, Urbana, IL 61801, USA; yjin31@illinois.edu
3 Aerospace Engineering, University of Illinois, Urbana, IL 61801, USA; hayat3@illinois.edu
4 Civil and Environmental Engineering, University of Illinois, Urbana, IL 61801, USA
* Correspondence: lpchamo@illinois.edu; Tel.: +1-217-300-7023

Received: 27 November 2017; Accepted: 28 December 2017; Published: 2 January 2018

Abstract: A wind-tunnel investigation was carried out to characterize the spatial distribution of the integral time scale (T^u) within, and in the vicinity of, two model wind farms. The turbine arrays were placed over a rough wall and operated under high turbulence. The two layouts consisted of aligned units distinguished only by the streamwise spacing (Δx_T) between the devices, set at five and ten rotor diameters d_T (or $S_x = \Delta x_T/d_T = 5$ and 10). They shared the same spanwise spacing between turbines of $2.5d_T$; this resulted in arrays of 8×3 and 5×3 horizontal-axis turbines. Hotwire anemometry was used to characterize the instantaneous velocity at various vertical and transverse locations along the central column of the wind farms. Results show that T^u was modulated by the wind farm layout. It was significantly reduced within the wind farms and right above them, where the internal boundary layer develops. The undisturbed levels above the wind farms were recovered only at $\approx d_T/2$ above the top tip. This quantity appeared to reach adjusted values starting the fifth row of turbines in the $S_x = 5$ wind farm, and earlier in the $S_x = 10$ counterpart. Within the adjusted zone, the distribution of T^u at hub height exhibited a negligible growth in the $S_x = 5$ case; whereas it underwent a mild growth in the $S_x = 10$ wind farm. In addition, the flow impinging the inner turbines exhibited $T^u/T^u_{inc} < 1$, where T^u_{inc} is the integral time scale of the overall incoming flow. Specifically, $T^u \to \beta T^u_{inc}$ at $z = z_{hub}$, where $\beta < 1$ within standard layouts of wind farms, in particular $\beta \approx 0.5$ and 0.7 for $S_x = 5$ and 10.

Keywords: integral time scale; wake; wind turbine; wind farm

1. Introduction

Installed power capacity from wind energy has been experiencing a monotonic increase worldwide in the last years; it accounted for almost half of all the electricity growth in 2015 [1], with large new installations of 30.75 GW in China [1]. Wind turbines operate under a variety of flow conditions characterized by long periods of high turbulence, which contain a broad range of energetic coherent motions. Understanding the distribution and dynamics of such flow structures is of paramount relevance to quantify the unsteady loading and power output fluctuations of wind turbines [2].

Early field measurements on full-scale 630 kW Nibe wind turbines made by Swift-Hook et al. [3] focused on the wake interaction between two turbines placed five rotor diameters apart; this information was used for the development and validation of various wind turbine wake models [4,5]. Field measurements of Milan et al. [6] showed the dominant role of the turbulence

structure on the power output of single turbines and wind farms. They suggested that power dynamics can be considered to follow adiabatic wind dynamics with a similar $f^{-5/3}$ spectral behavior for time scales larger than the regulating time of control systems. Power measurements on a full-scale 2.5 MW wind turbine by Chamorro et al. [7] showed that power fluctuations are strongly modulated by the scales of turbulence in a complex way. They suggested that the spectral content of the power fluctuations, Φ_P, and that of the incoming flow, Φ_u, exhibit a relationship that can be characterized by a nonlinear transfer function $G(f) \propto f^{-2}$ across relevant length scales. Recently, Tobin et al. [8] introduced a tuning-free model for such transfer function $G(f)$ for single turbines, which was tested across turbine sizes. Overall, this implies that accurate estimation of Φ_u is essential for the estimation of the corresponding structure of the power fluctuations of wind turbines. Various models have been proposed to estimate this quantity (e.g., [9,10]), where the turbulence levels (σ_u) and integral time scale (T^u) [11] are key bulk parameters. In the context of wind farms, power fluctuations of wind turbines can be estimated via Φ_u and $G(f)$ using local incoming flow to each turbine. This is possible with a quantitative description of the spatial distribution of σ_u and T^u within wind farms. Even though turbulence levels within wind farms have been characterized in laboratory (e.g., [12–14]), field experiments (e.g., [15,16]) and numerical simulations (e.g., [17–21]) as well as through analytical models for single turbine wakes (e.g., [22–24]), equivalent characterization for T^u is very limited. Within the understanding the turbulence structure of wake flows, Lundquist and Bariteau [25] quantified the turbulence dissipation in the wake of a full-scale wind turbine, owing to the coupling between small-scale and large-scale structures and the turbulence dissipation rate in the wake [26].

Recently, Jin et al. [27] analyzed the distribution of the large-scale motions and integral length scale (Λ_u) in the wake of a wind turbine within a uniform flow under very low and high turbulence levels. They showed the distinctive effects of background turbulence on Λ_u in the intermediate and far field wake; however, its growth rate was approximately linear regardless of the background turbulence. Chamorro et al. [28] proposed an approach to quantify a wake flow recovery, which is based on the development of integral length scale along the wake centerline. They also reported that the evolution of Λ_u is roughly independent of the turbine tip–speed ratio. Furthermore, Singh et al. [29] pointed out that wind turbines reduce the intermittency and asymmetry in the wake by breaking and deflecting the large-scale flow structures; the non-local transfer between large and small scales is strongly attenuated, resulting in the more homogenized velocity structure as compared to the base flow. Numerical simulations by Blackmore et al. [30] showed that the increase in Λ_u of the incoming flow might speed up the wake recovery and increase the wake span.

Despite the various efforts to characterize the flow around turbines, the distribution of large scale motions and, in particular T^u or Λ_u, within wind farms has not been characterized in detail. Quantification of the spatial distribution of T^u within turbine arrays is essential for analytical models for predicting power output fluctuations. Consequently, understanding this phenomenon is instrumental to optimize the operation of wind farms and improve operation of power grids, among others. In this experimental study, we inspect the spatial distribution of this quantity in the vicinity of two model wind farm layouts with Cartesian configuration. Section 2 describes the experimental setup; Section 3 presents the results and discussion. Main remarks are summarized in Section 4.

2. Experimental Setup

A laboratory experiment was performed in the Eiffel-type boundary-layer wind tunnel of the University of Illinois at Urbana-Champaign's Renewable Energy and Turbulent Environment Group. The wind tunnel has a test section of approximately 6.1 m long, 0.91 m wide, and 0.45 m high (see Figure 1a). The wind-tunnel ceiling is fully adjustable to control the pressure gradient along the test section, which was set to nearly zero during these experiments. More details of the facility can be found in Adrian et al. [31].

Two miniature wind farms were placed and operated under high incoming turbulence, which was induced with an active turbulence generator located at the entrance of the test section. The turbulence

generator has horizontal and vertical rods, separately driven by an electric stepper motor, and rotated at a frequency of 0.1 Hz with random changes in the direction; additional information of the turbulence generator can be found in Jin et al. [27]. The resulting structure of the turbulence contained a well-developed inertial subrange that spanned two decades. A surface roughness consisting of 5 mm thick chains laid in the spanwise direction every 0.2 m between chains [32] was added along the test section. The resulting turbulent boundary layer of the incoming flow had a well-defined log region with a friction velocity of $u_* \approx 0.55$ ms^{-1}, an aerodynamic roughness length of $z_o \approx 0.12$ mm and a thickness of $\delta/z_{hub} \approx 2.2$, where $z_{hub} = 125$ mm is the hub height of the turbines. A similar roughness configuration was used in wind tunnel experiments by Ohya [33] and Chamorro et al. [32] to study stable boundary layers and wind turbine wakes over rough surfaces, respectively. Figure 1b shows vertical profiles of the mean velocity U/U_{hub}, turbulence intensity $I_u = \sigma_u/U_{hub}$ and integral time scale $T^u_{inc}U_{hub}/d_T$ of the incoming flow, and also included selected velocity spectra at hub height Φ_u (incoming flow, and $3d_T$ downwind of the 1st and 5th rows). Here, $U_{hub} = 9.33$ ms^{-1} and $d_T = 120$ mm are the incoming velocity at hub height and rotor diameter, whereas σ_u is the standard deviation of the streamwise velocity fluctuations. The incoming flow at hub height has a $T^u_{inc}(z = z_{hub}) \approx 1.3U_{hub}/d_T$, which is equivalent to an integral length scale $\Lambda^u_{inc}(z = z_{hub}) \approx 1.3d_T$.

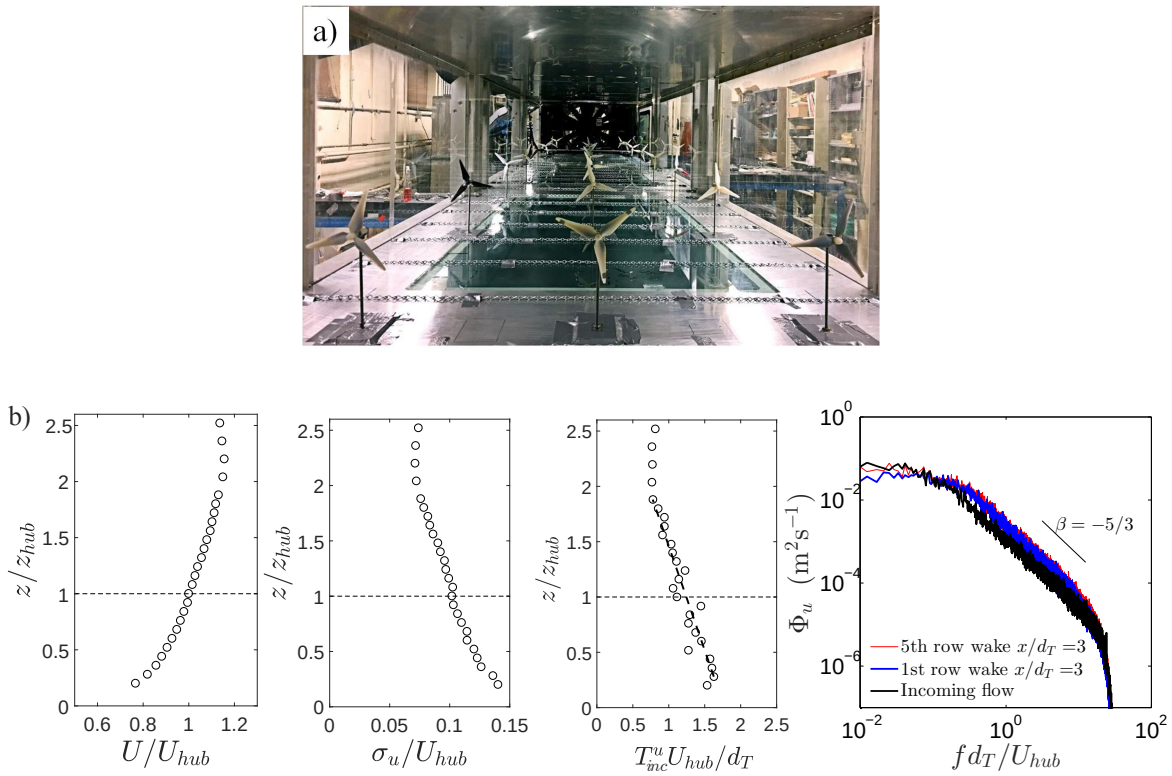

Figure 1. (**a**) photograph of one of the model wind farms in the test section of the wind tunnel; (**b**) incoming boundary layer statistics: time-averaged streamwise velocity profile U/U_{hub}, turbulence intensity σ_u/U_{hub}, integral time scale $T^u_{inc}U_{hub}/d_T$ and velocity spectra at hub height Φ_u (incoming flow, and $3d_T$ downwind of the first and fifth rows). $U_{hub} = 9.33$ ms^{-1} and $T^u_{inc}(z = z_{hub}) \approx 1.3d_T/U_{hub} \approx 1.7 \times 10^{-2}$ s.

The turbine rotors were 3D printed from Objet Vero material at University of Illinois rapid-prototyping laboratory. The geometry of the representative rotor is based on a reference model turbine designed at Sandia National Laboratory [34,35]. A Precision Microdrive 112-001 Micro Core 12 mm Direct Current (DC) motor acted as the loading system, which resulted in a rated power $P_0 \sim 1$ W [8,36]; additional information on the model turbine can be found in Tobin et al. [37]. The two

wind farm layouts consisted of aligned turbines with streamwise separation of $S_x = \Delta x_T/d_T = 5$ and 10, which shared the same spanwise separation of $S_y = \Delta y/d_T = 2.5$. This resulted in two arrays of 8×3 and 5×3 turbines. The last row was omitted from the present results to avoid boundary effects. For these layouts, the incoming Reynolds number was $Re = U_{hub}d_T/\nu \approx 7.5 \times 10^4$, and rotor tip–speed ratio of $\lambda = \omega d_T/(2U_{hub}) \approx 4.9$, where ν is the kinematic viscosity of air and ω is the angular velocity of the rotor.

Single-point velocity measurements were obtained at various locations with a hotwire anemometer. It was calibrated against a pitot-static probe in the freestream region of the wind tunnel in the absence of the turbulence generator. The calibration was performed at the beginning and the end of the experiments to ensure negligible voltage drift of the data acquisition system. A 2D Velmex traversing system allowed automatic motions of the probe in the spanwise and vertical directions. The anemometer was positioned downwind of each of the central turbines every $\Delta x/d_T = 0.5$ and 1 for the $S_x = 5$ and 10 layouts. At each of these streamwise locations, velocity profiles were taken at the central plane ($y = 0$) for heights ranging from $z = 25$ mm to $z = 225$ mm (i.e., $z/z_{hub} = 0.2$ to 1.8) every $\Delta z = 10$ mm ($\Delta z/z_{hub} = 0.08$) and from $z = 225$ mm to $z = 305$ mm (i.e., $z/z_{hub} = 1.8$ to 2.44) every $\Delta z = 20$ mm ($\Delta z/z_{hub} = 0.16$). See Figure 2a. Complementary wall-parallel measurements were taken within the plane $z = z_{hub}$ for a spanwise range $y \in [-120,\ 120]$ mm (i.e., $y/d_T = [-1, 1]$) every $\Delta y = 10$ mm along the same streamwise locations as those of the vertical profiles. See Figure 2b. The hotwire was connected to a Dantec dynamic system, which sampled the sensor voltage signatures at 10 kHz for measurement periods of 120 s. Throughout the calibration and experiments, the room temperature was kept at 23 ± 0.5 °C to avoid thermal drift of the voltage signals.

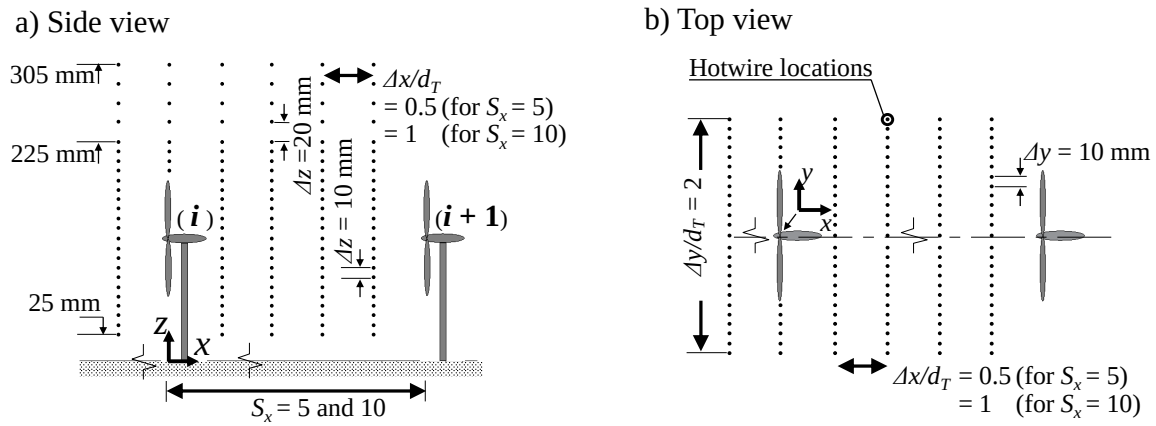

Figure 2. (**a**) Detail of the hotwire measurement locations in a vertical plane within representative rows i and $i + 1$; (**b**) same as (**a**) but within a wall-parallel plane at hub height.

3. Results and Discussion

The integral time scale T^u at the given location is computed via the integral of the autocorrelation function of the streamwise velocity $r(\tau)$, as follows:

$$r(\tau) = \overline{u'(t)\,u'(t-\tau)}/\sigma_u^2, \tag{1}$$

$$T^u = \int_0^\infty r(\tau)\,d\tau, \tag{2}$$

where τ is the time lag, u' is the streamwise velocity fluctuations and σ_u^2 is the corresponding velocity variance. For practical purposes, the integral in Equation (2) is evaluated up to a time lag where $r(t)$ is sufficiently low [28]; here, it is set at $r = 0.05$ in all interrogated locations.

3.1. Vertical Distribution of the Integral Time Scale

Iso-contours of $T^u(x, y = 0, z)/T^u_{inc}(z)$ in the vertical plane coincident with the axis of the turbines at the center of the wind farms for the cases $S_x = 5$ and $S_x = 10$ are illustrated in Figure 3. As expected, T^u is substantially reduced within the wind farms, which also occurs right above the top tip as a result of the development of an internal boundary layer. Like the momentum or turbulence levels, this quantity also offers an alternative way to characterize the flow development inside a wind farm. Indeed, note that the distribution of T^u in the wind farm with $S_x = 5$ reaches an apparent equilibrium starting the wake of the fifth row of turbines. There, the downwind turbines are impinged by a flow with $T^u/T^u_{inc} \approx 0.5$ in most of the rotor. Note, however, that this is not the case for the wind farm with $S_x = 10$; there, the distribution is roughly adjusted starting the third row of turbines with $T^u/T^u_{inc} \approx 0.7$ in the vicinity of those rotors. The substantially larger spacing between turbines allows better entrainment from the top, and the development of the turbulence structure. In addition, the entrainment process from the top leads to a relatively asymmetric distribution of T^u with larger values towards the top tip.

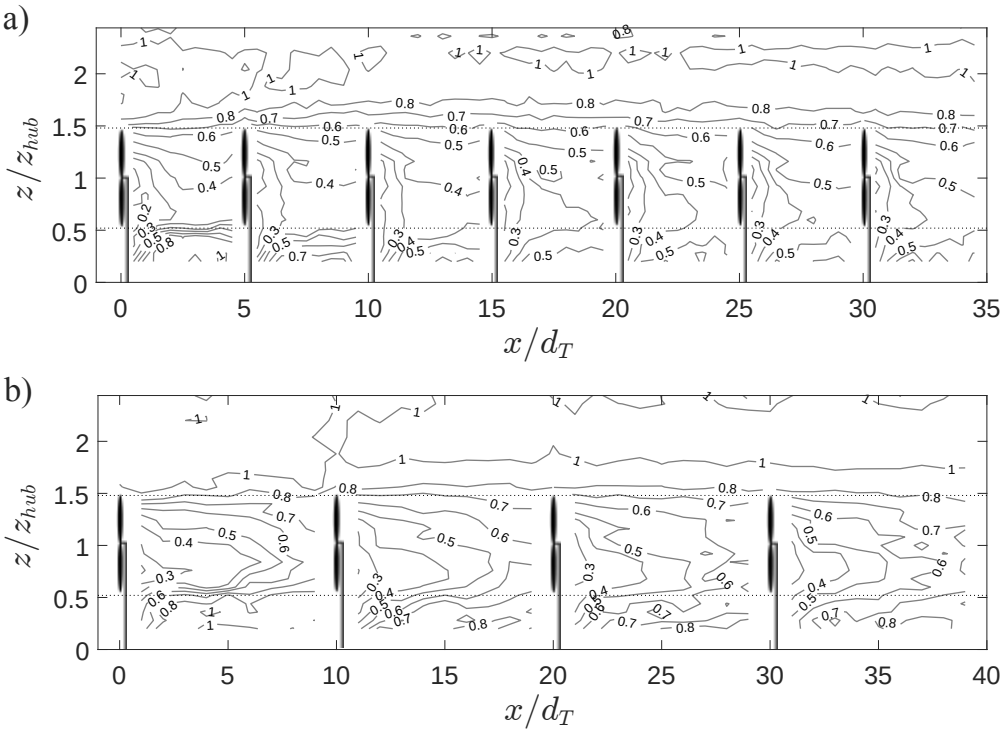

Figure 3. Isocontours of the normalized integral Time scale $T^u(x, y = 0, z)/T^u_{inc}(z)$ within a vertical plane along the central column of the wind farms. (**a**) $S_x = 5$; (**b**) $S_x = 10$. The two horizontal dotted lines mark the location of turbine top and bottom tips.

To further illustrate the evolution of T^u, selected profiles at the hub height ($z/z_{hub} = 1$), at the top tip ($z/z_{hub} \approx 1.5$) and a radius above the top tip of the wind farms ($z/z_{hub} \approx 2$) are shown across the streamwise distance in Figure 4 for the two layouts. The profiles are superimposed to illustrate the effect of the turbine spacing at various heights. At $z/z_{hub} = 1$, the magnitude and growth rate of T^u appear roughly insensitive up to $S_x < 5$ (Figure 4a). In contrast, T^u significantly differ at the top tip of the wind farms; this quantity is consistently larger in the $S_x = 10$ across x/d_T (Figure 4b). This indicates that the internal boundary layer developed right above the wind farms exhibits a turbulence structure that is strongly affected by the layout. Interestingly, T^u also exhibits a clear growth with x/d_T from the second row of turbines in the $S_x = 5$ layout. As expected, such growth is locally interrupted right behind each turbine. In light of the results at the hub height, the structural changes of the turbulence

appear to mostly have an impact around the top tip. Further above, the effects of the layout and turbines in the evolution of T^u become gradually reduced. This is illustrated in Figure 4c at $z/z_{hub} = 2$.

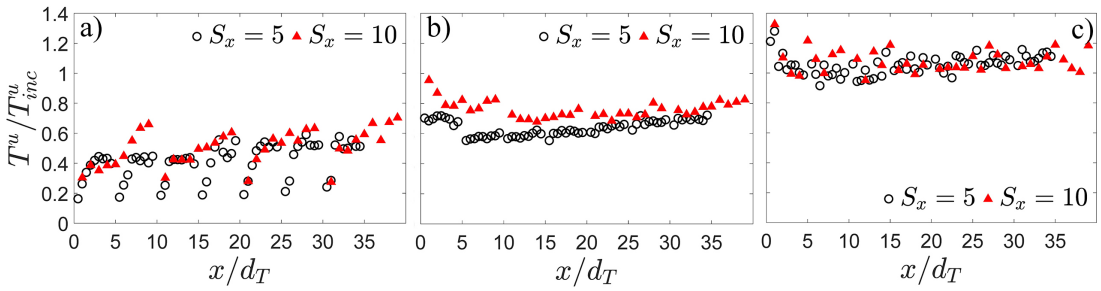

Figure 4. Normalized integral Time scale $T^u(x, y = 0, z)/T^u_{inc}(z = z_{hub})$ along the central column of the wind farms. (**a**) at the hub height ($z/z_{hub} = 1$); (**b**) at the top tip ($z/z_{hub} \approx 1.5$); (**c**) a radius over the top tip ($z/z_{hub} \approx 2$).

The representative log-log evolution of T^u for the adjusted rows at $z/z_{hub} = 1$ along the rotor axis is illustrated in Figure 5. It exhibits negligible increase past $x/d_T \geq 2$ in the $S_x = 5$. This is not the case in the $S_x = 10$ layout, where T_u undergoes a modest monotonic growth ($T^u/T^u_{hub} \propto (x/d_T)^a, a \sim 0.24$ with a correlation coefficient ≈0.74). Note the higher $\partial(T^u/T^u_{hub})/\partial(x/d_T)$ in the very near wake, namely $x/d_T \leq 2$. This particular behavior was noted by Jin et al. [27] in the wake of a single turbine under uniform flow with very low incoming turbulence and negligible integral scale. They also noted that such phenomenon is not present when the turbine was operated under high turbulence ($I_u = 11.5\%$) with large $T^u_{inc}(z = z_{hub})U_{hub}/d_T$ ($= 2.5$). Here, the turbines within the adjusted region are exposed to intermediate $T^u_{inc}(z = z_{hub})$ and $\partial(T^u/T^u_{hub})/\partial(x/d_T)$ with respect to the cases with single turbine wake under negligible and high turbulence. This is, consequently, consistent with those measurements. For practical purposes, however, T^u trends in the intermediate and far wakes are of interest; in particular, those impinging the turbines within wind farms. Extrapolation of Figure 5 suggests that, for common spacing of wind turbines within wind farms, T^u levels are likely lower than that of the global incoming flow.

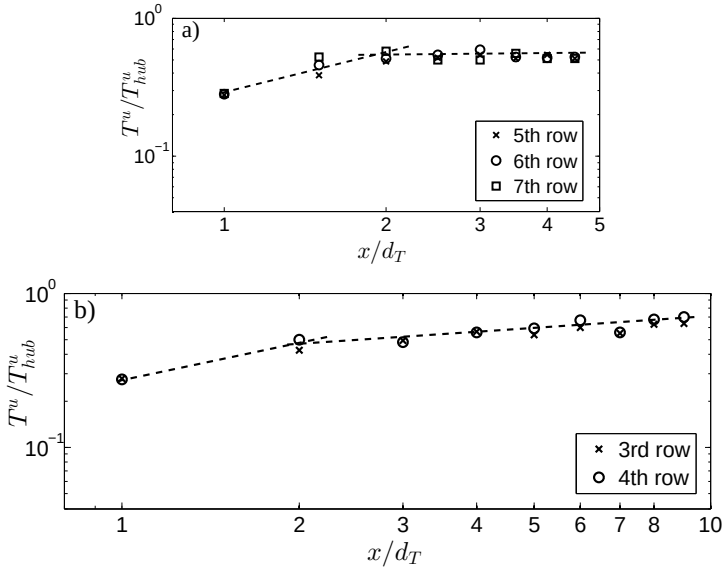

Figure 5. Log-log distribution of the normalized integral time scale T^u/T^u_{inc} at $z = z_{hub}$ along the rotor axes in the adjusted rows. (**a**) $S_x = 5$; (**b**) $S_x = 10$.

3.2. Wall-Parallel Distribution of the Integral Time Scale

For completeness, isocontours of T^u/T^u_{inc} within the wall-parallel plane $z/z_{hub} = 1$ are shown in Figure 6 for both $S_x = 5$ and $S_x = 10$ wind-farm layouts. The region considered in each case include a transverse range between $y/d_T = [-1,\ 1]$ with respect to the central row of wind turbines. It reveals that T^u is roughly symmetric with respect to the central axis $y = 0$, and the values of T^u impinging each rotor are consistent with those obtained from the vertical profiles. Similar to the internal boundary layer above the wind farms, T^u undergoes similar phenomenon laterally. This implies that the flow within wind–turbine arrays with reduced lateral spacing may have T^u lower than that of the incoming flow. Due to the lateral flow development, $T^u/T^u_{inc}|_{z=z_{hub}}$ converges to ∼0.6 and ∼0.7 in the outer vicinity of the lateral tips for the $S_x = 5$ and 10 cases, respectively.

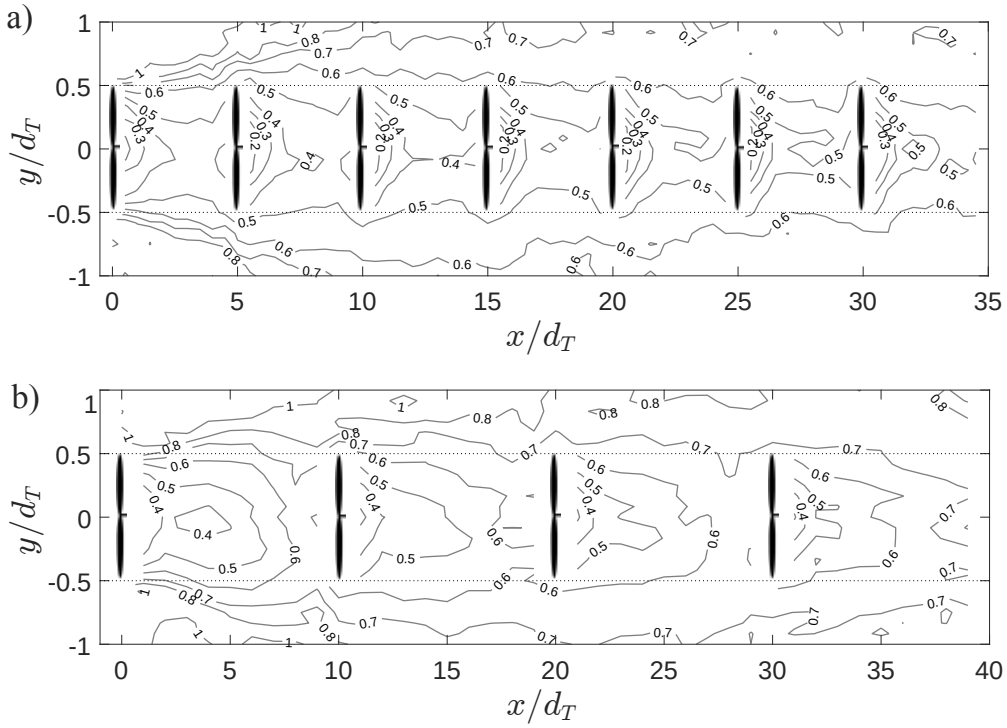

Figure 6. Isocontours of the normalized integral time scale $T^u(x, y, z = z_{hub})/T^u_{inc}(z = z_{hub})$ within a wall-parallel plane along the central column of the wind farms. (**a**) $S_x = 5$; (**b**) $S_x = 10$. The two horizontal dotted lines mark the location of turbines' lateral tips.

Finally, the compensated velocity spectra $f\Phi_u$ at $z/z_{hub} = 1$ along the rotor axes is shown in Figure 7 to illustrate the distribution of the contributing turbulent motions across scales. Enhanced levels of $f\Phi_u$ are mostly contained within the spectral region defined by the reduced frequency $fd_T/U_{hub} \sim [10^{-1}, 10^0]$ with larger values around $x/d_T \sim [2, 4]$. Within this spatial region, the tip vortices lose coherence and the shear layer enhances a multiscale mixing across the span reaching the wake axis, which is reflected in the distribution of the compensated energy content of $f\Phi_u$. The increased levels of $f\Phi_u$ in the scales larger than the rotor ($fd_T/U_{hub} < 10^0$) reveal a strong modulation of the wake on the power output fluctuations of the turbines. Figure 7 also show the influential effect of the layout on the turbulence impinging the turbines within wind farms and, therefore, power output fluctuations at the wind-farm scale ($\Phi_{p_{wf}}$). Here, the local velocity spectrum is essential for estimating $\Phi_{p_{wf}}$. Indeed, the structure of the turbulence-driven power fluctuations of a $M \times N$ wind farm (M and N refer to the number of columns in the transverse and streamwise directions) was recently explored by Liu et al. [38]. They proposed a model that takes into account the

turbulent interaction between the flow and turbines, and the advection between turbine pairs. It is given as follows:

$$\Phi_{p_{wf}} = M\sum_{i=1}^{N}\Phi_{p_i} + 2M\sum_{i=1}^{N}\sum_{j>i}^{N}\Phi_{p_j} cos\left(2\pi f\tau_{ij}\right) \times \exp\left(-\frac{2}{3}\pi^2 f^2 {\tau_{ij}}^2 {I_j}^2\right), \quad (3)$$

where $\tau_{ij} = (j-i)S_x d_T/U_j$ represents the advection time between turbines i and j, and I_j denotes the local turbulence intensity I_u of the turbine j. The building block of $\Phi_{p_{wf}}$ (Equation (3)) is the local power output spectrum Φ_{Pi}, which can be estimated from the velocity spectrum via transfer function as $\Phi_P \propto G(f)\Phi_u$ [7]. Tobin et al. [8] proposed a tuning-free model for $G(f)$ and suggested using the von Kármán model for Φ_u [10], which is defined as:

$$\Phi_P(f) = G(f)\Phi_u = \frac{3/2 C_P \rho A U_{hub}^2}{\sqrt{1+(2\pi t_i)^4}} \times \frac{4\sigma_u^2 T^u}{\left(1+70.8\left(fT^u\right)^2\right)^{5/6}}. \quad (4)$$

Here, C_P is the power coefficient, ρ is the air density, A is the swept area of the turbine rotor and t_i is the inertial timescale [8]. An example of the measured Φ_P of the turbine in the first row is illustrated in Figure 8; it also includes Φ_u and $G(f)$ for reference to visually understand the distinctive power–law trends of Φ_P. Within wind farms, Equation (4) can be used to estimate $\Phi_P(f) \rightarrow \Phi_{Pi}$ with $T^u \rightarrow \beta T^u_{inc}$ at $z = z_{hub}$. Our study indicates that $\beta < 1$ within standard layouts of wind farms; in particular, $\beta \approx 0.5$ and 0.7 for $S_x = 5$ and 10.

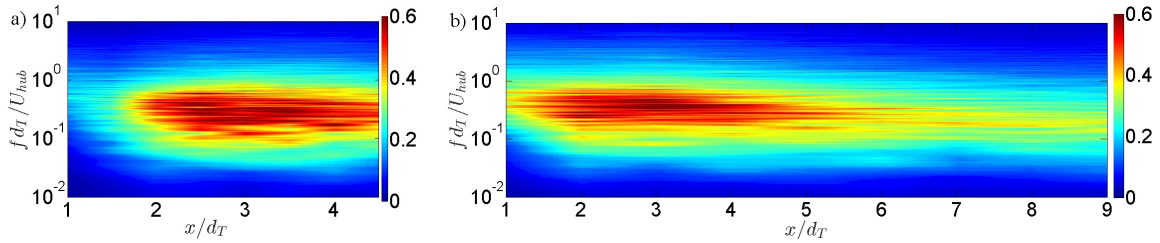

Figure 7. Compensated velocity spectra $f\Phi_u$ at $z/z_{hub} = 1$ along the rotor axis in the adjusted rows (shown the last row in each layout). (**a**) $S_x = 5$; (**b**) $S_x = 10$.

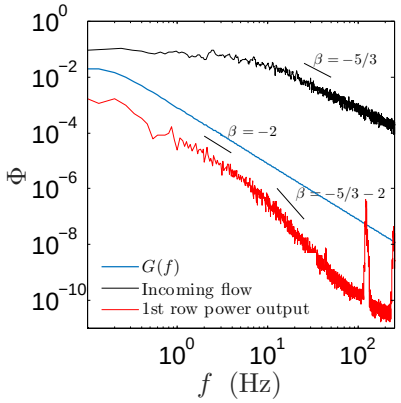

Figure 8. Spectra of the incoming flow at hub height $\Phi_u(z = z_{hub})$ (black), and turbine output power of the first row Φ_p (red). The transfer function of the turbine $G(f)$ is included as a reference; it allows a visual understanding of the distinctive power–law trends of Φ_p.

4. Conclusions

Understanding the distribution of the integral time scale within wind farms is the key to estimating the spectral features of the flow impinging the inner turbines. Such information is particularly useful to predict power fluctuations of individual turbines and, consequently, those at wind-farm scale. The experimental inspection of the flow within, and in the vicinity of, two model wind farms revealed strong modulation of the wind farm layout on T^u. It also defined the location where adjusted values are reached, which provides an alternative way to assess the turbulence development in large turbine arrays. T^u impinging inner turbines underwent significant reduction with respect to that of the incoming flow as a result of the dampening of the very large-scale motions. The results indicate that $T^u \rightarrow \beta T^u_{inc}$ at $z = z_{hub}$, where $\beta < 1$; in particular, $\beta \approx 0.5$ and 0.7 for $S_x = 5$ and 10. This quantity used in the context of Equations (3) and (4) provides a robust estimation of the structure of the power fluctuations at wind-farm scale.

Acknowledgments: This work was supported by the Department of Mechanical Science and Engineering, University of Illinois at Urbana-Champaign, as part of the start-up package of Leonardo P. Chamorro. The authors are very grateful to the National Science Foundation, Grant No. ECCS-1610897, for funding this research. The authors also acknowledge the China Scholarship Council for supporting Huiwen Liu's research abroad.

Author Contributions: Huiwen Liu performed the experiments, processed the data and drafted the manuscript; Imran Hayat helped with the experiments, and Yaqing Jin helped with the analysis; Leonardo P. Chamorro defined the concept, analysis and helped to write the manuscript.

Conflicts of Interest: The authors declare no conflict of interest.

References

1. Global Wind Energy Council (GWEC). *Global Wind Report Annual Market Update*; GWEC: Brussel, Belgium, 2015.
2. Vermeer, L.J.; Sørenson, J.N.; Crespo, A. Wind turbine wake aerodynamics. *Prog. Aerosp. Sci.* **2003**, *39*, 467–510.
3. Swift-Hook, D.; Hojstrup, J.; McIntosh, D.; Milborrow, D.; Taylor, G. Nibe wake measurements project in Denmark. In Proceedings of the European Wind Energy Conference, Hamburg, Germany, 22–26 October 1984; pp. 22–28.
4. Jensen, N.O. *A Note on Wind Generator Interaction;* Risø-M; No. 2411; Technical University of Denmark: Lyngby, Denmark, 1983.
5. Katic, I.; Højstrup, J.; Jensen, N.O. A simple model for cluster efficiency. In Proceedings of the European Wind Energy Association Conference and Exhibition, Rome, Italy, 7–9 October 1986; pp. 407–410.
6. Milan, P.; Wächter, M.; Peinke, J. Turbulent character of wind energy. *Phys. Rev. Lett.* **2013**, *110*, 138701.
7. Chamorro, L.P.; Lee, S.J.; Olsen, D.; Milliren, C.; Marr, J.; Arndt, R.E.A.; Sotiropoulos, F. Turbulence effects on a full–scale 2.5 MW horizontal–axis wind turbine under neutrally stratified conditions. *Wind Energy* **2015**, *18*, 339–349.
8. Tobin, N.; Zhu, H.; Chamorro, L.P. Spectral behaviour of the turbulence-driven power fluctuations of wind turbines. *J. Turbul.* **2015**, *16*, 832–846.
9. Kaimal, J.; Finnigan, J. *Atmospheric Boundary Layer Flows—Their Structure and Measurement*; Oxford University Press: New York, NY, USA, 1994.
10. Von Karman, T. Progress in the statistical theory of turbulence. *Proc. Natl. Acad. Sci. USA* **1948**, *34*, 530–539.
11. Pope, S.B. *Turbulent Flows*; Cambridge University Press: Cambridge, UK, 2001.
12. Chamorro, L.P.; Sotiropoulos, F. Turbulent flow inside and above a wind farm: A wind-tunnel study. *Energies* **2011**, *4*, 1916–1936.
13. Markfort, C.D.; Zhang, W.; Porté-Agel, F. Turbulent flow and scalar transport through and over aligned staggered wind farms. *J. Turbul.* **2012**, *13*, 1–36.
14. Newman, J.; Lebron, J.; Meneveau, C.; Castillo, L. Streamwise development of the wind turbine boundary layer over a model wind turbine array. *Phys. Fluids* **2013**, *25*, 085108.

15. Hong, J.; Toloui, M.; Chamorro, L.P.; Guala, M.; Howard, K.; Riley, S.; Sotiropoulos, F. Natural snowfall reveals large-scale flow structures in the wake of a 2.5-MW wind turbine. *Nat. Commun.* **2014**, *5*, 4216, doi:10.1038/ncomms5216.
16. Machefaux, E.; Larsen, G.C.; Koblitz, T.; Troldborg, N.; Kelly, M.C.; Chougule, A.; Hansen, K.S.; Rodrigo, J.S. An experimental and numerical study of the atmospheric stability impact on wind turbine wakes. *Wind Energy* **2016**, *19*, 1785–1805.
17. Lu, H.; Porté-Agel, F. Large-eddy simulation of a very large wind farm in a stable atmospheric boundary layer. *Phys. Fluids* **2011**, *23*, 065101.
18. Meyers, J.; Meneveau, C. Optimal turbine spacing in fully developed wind farm boundary layers. *Wind Energy* **2012**, *15*, 305–317.
19. Yang, D.; Meneveau, C.; Shen, L. Large-eddy simulation of offshore wind farm. *Phys. Fluids* **2014**, *26*, 025101.
20. Wu, Y.T.; Porté-Agel, F. Modeling turbine wakes and power losses within a wind farm using LES: An application to the Horns Rev offshore wind farm. *Renew. Energy* **2015**, *75*, 945–955.
21. Stevens, R.J.; Gayme, D.F.; Meneveau, C. Effects of turbine spacing on the power output of extended wind-farms. *Wind Energy* **2016**, *19*, 359–370.
22. Larsen, G.C.; Højstrup, J.; Madsen, H.A. Wind fields in wakes. In Proceedings of the 1996 European Wind Energy Conference and Exhibition, Goteborg, Sweden, 20–24 May 1996; HS Stephens & Associates: Bedford, UK, 1996; pp. 764–768.
23. Crespo, A.; Hernandez, J. Analytical correlations for turbulence characteristics in the wakes of wind turbines. In Proceedings of the European Community Wind Energy Conference, Travemuende, Germany, 8–12 March 1993; pp. 8–12.
24. Crespo, A.; Herna, J. Turbulence characteristics in wind turbine wakes. *J. Wind Eng. Ind. Aerodyn.* **1996**, *61*, 71–85.
25. Lundquist, J.; Bariteau, L. Dissipation of Turbulence in the Wake of a Wind Turbine. *Bound.-Layer Meteorol.* **2015**, *154*, 229–241.
26. Hamilton, N.; Suk Kang, H.; Meneveau, C.; Bayoán Cal, R. Statistical analysis of kinetic energy entrainment in a model wind turbine array boundary layer. *J. Renew. Sustain. Energy* **2012**, *4*, 063105.
27. Jin, Y.; Liu, H.; Aggarwal, R.; Singh, A.; Chamorro, L.P. Effects of Freestream Turbulence in a Model Wind Turbine Wake. *Energies* **2016**, *9*, 830.
28. Chamorro, L.; Hill, C.; Morton, S.; Ellis, C.; Arndt, R.; Sotiropoulos, F. On the interaction between a turbulent open channel flow and an axial-flow turbine. *J. Fluid Mech.* **2013**, *716*, 658–670.
29. Singh, A.; Howard, K.B.; Guala, M. On the homogenization of turbulent flow structures in the wake of a model wind turbine. *Phys. Fluids* **2014**, *26*, 025103.
30. Blackmore, T.; Batten, W.M.J.; Bahaj, A.S. Influence of turbulence on the wake of a marine current turbine simulator. *Proc. R. Soc. A* **2014**, *470*, 20140331.
31. Adrian, R.; Meinhart, C.; Tomkins, C. Vortex organization in the outer region of the turbulent boundary layer. *J. Fluid Mech.* **2000**, *422*, 1–54.
32. Chamorro, L.P.; Porté-Agel, F. A Wind-Tunnel Investigation of Wind-Turbine Wakes: Boundary-Layer Turbulence Effects. *Bound.-Layer Meteorol.* **2009**, *132*, 129–149.
33. Ohya, Y. Wind-tunnel study of atmospheric stable boundary layers over a rough surface. *Bound.-Layer Meteorol.* **2001**, *98*, 57–82.
34. Johnson, E.; Fontaine, A.A.; Jonson, M.L.; Meyer, R.S.; Straka, W.A.; Young, S.; van Dam, C.; Shiu, H.; Barone, M. A1: 8.7 scale water tunnel test of an axial flow water turbine. In Proceedings of the 1st Marine Energy Technology Symposium (METS13), Washington, DC, USA, 10–11 April 2013.
35. Shiu, H.; van Dam, C.; Johnson, E.; Barone, M.; Phillips, R.; Straka, W.; Fontaine, A.; Jonson, M. A design of a hydrofoil family for current-driven marine-hydrokinetic turbines. In Proceedings of the 20th International Conference on Nuclear Engineering and the American Society of Mechanical Engineers 2012 Power Conference, Anaheim, CA, USA, 30 July–3 August 2012; pp. 839–847.
36. Tobin, N.; Hamed, A.M.; Chamorro, L.P. Fractional Flow Speed-Up from Porous Windbreaks for Enhanced Wind-Turbine Power. *Bound.-Layer Meteorol.* **2017**, *163*, 253–271, doi:10.1007/s10546-016-0228-8.

37. Tobin, N.; Hamed, A.M.; Chamorro, L.P. An Experimental Study on the Effects of Winglets on the Wake and Performance of a Model Wind Turbine. *Energies* **2015**, *8*, 11955–11972.
38. Liu, H.; Jin, Y.; Tobin, N.; Chamorro, L.P. Towards uncovering the structure of power fluctuations of wind farms. *Phys. Rev. E* **2017**, *96*, 063117.